Molecules and Cells

Necroptosis Is a Mechanism of Death in Mouse Induced Hepatocyte-Like Cells Reprogrammed from Mouse Embryonic Fibroblasts

Yun-Suk Lee[1], Kyung-Mee Park[2], Lina Yu[3], Ho-Hyun Kwak[3], Hee-Jun Na[1], Kyung-Sun Kang[4], and Heung-Myong Woo[3,*]

[1]Hauul Bio Incorporation, Chuncheon 24398, Korea, [2]College of Veterinary Medicine, Chungbuk National University, Cheongju, Chungbuk 28644, Korea, [3]College of Veterinary Medicine, Kangwon National University, Chuncheon 24341, Korea, [4]Adult Stem Cell Research Center, College of Veterinary Medicine, Seoul National University, Seoul 08826, Korea
*Correspondence: woohm@kangwon.ac.kr
http://dx.doi.org/10.14348/molcells.2018.2353
www.molcells.org

Liver transplantation is recommended for patients with liver failure, but liver donors are limited. This necessitates the development of artificial livers, and hepatocytes are necessary to develop such artificial livers. Although induced hepatocyte-like cells are used in artificial livers, the characteristics of mouse induced hepatocyte-like cells (miHeps) reprogrammed with embryonic fibroblasts have not yet been clarified. Therefore, this study investigated the mechanisms underlying the survival, function, and death of miHeps. miHeps showed decreased cell viability, increased cytotoxicity, decreased hepatic function, and albumin and urea secretion at passage 14. Addition of necrostatin-1 (NEC-1) to miHeps inhibited necrosome formation and reactive oxygen species generation and increased cell survival. However, NEC-1 did not affect the hepatic function of miHeps. These results provide a basis for development of artificial livers using hepatocytes.

Keywords: artificial liver, mouse induced hepatocyte-like cells, necroptosis, necrostatin-1, necrosome formation

INTRODUCTION

The best treatment for patients with end-stage liver disease is liver transplantation (Dienstag and Cosimi, 2012; Ho et al., 2016; Zarrinpar and Busuttil, 2013). The number of patients waiting for liver transplants and those dying without surgery is rapidly increasing (Dasarathy, 2012; Hannoun et al., 2016). Therefore, it is necessary to develop an organ alternative, and various methods such as tissue engineering, three-dimensional (3D) printer technology, and stem cell restoration for artificial organs are under investigation (Leberfinger et al., 2017; Sakiyama et al., 2017).

Hepatocytes that can be used in artificial livers include progenitor cells, hepatocytes derived from induced pluripotent stem cells (iPSCs), induced hepatocyte-like cells (iHeps), primary hepatic cells, and immortalized hepatocyte cell lines (Wang et al., 2017). Ideally, the cells should be easy to acquire, elicit no immune response, multiply rapidly, differentiate into hepatocytes, and raise no ethical concerns. iHeps are easy to acquire and differentiate into hepatocytes (Wang et al., 2017). Mouse induced hepatocyte-like cells (miHeps) are reprogrammed with mouse embryonic fibroblasts by the pMX retroviral method, and they express the hepatic transcription factors hepatocyte nuclear factor 4 alpha (HNF4α) and forkhead box protein A3 (FOXA3) (Kang et al., 2017). However, the characteristics of miHeps remain unclear.

Cell death can occur through either apoptosis or necroptosis (Cho and Park, 2017). Apoptosis is molecularly activated by the caspase cascade, and Z-VAD-FMK is a well-known

Received 10 December, 2017; revised 13 May, 2018; accepted 5 June, 2018; published online 10 July, 2018

eISSN: 0219-1032

apoptosis inhibitor (Masuoka et al., 2009). Necroptosis induces necrosome formation via interaction between receptor-interacting protein kinase 1 (RIP1) and RIP3. Phosphorylated RIP3 phosphorylates mixed-lineage kinase domain-like (MLKL), and necrostatin-1 (NEC-1) is a well-known necroptosis inhibitor (Cho, 2014). Moreover, reactive oxygen species (ROS) can promote necroptosis in hepatocytes.

In this study, we investigated the mechanisms underlying the survival, proliferation, function, and cell death of miHeps, and confirmed necroptosis by necrosome formation via binding with RIP1 and RIP3 in miHeps. Therefore, the aim of this study was to determine the characteristics of induced hepatocyte-like cells for use in artificial livers.

MATERIALS AND METHODS

Cell culture

miHeps obtained from the College of Medicine, Hanyang University, Seoul, Korea, were cultured on 0.1% gelatin plates with 10% fetal bovine serum (FBS; Thermo Fisher Scientific, USA), 1× glutamax (Thermo Fisher Scientific), 10 mM nicotinamide (Sigma-Aldrich, USA), 50 μM β-mercaptoethanol (Sigma-Aldrich), 1× antibiotic-antimycotic (Thermo Fisher Scientific), 20 ng/ml hepatocyte growth factor (Peprotech, USA), 20 ng/ml epidermal growth factor (Peprotech), 1,000× dexamethasone (Sigma-Aldrich), and 1× insulin-transferrin-sodium (Thermo Fisher Scientific)-supplemented Dulbecco's modified Eagle's medium: nutrient mixture F-12 (DMEM/F12) (WelGENE Biotech, Korea). SV40-immortalized mouse hepatocytes (msHeps) were grown at 37℃ in 5% CO_2 in PriGrow II culture medium (Abcam, USA) supplemented with 10% FBS and antibiotics (Thermo Fisher Scientific).

Chemical compounds

NEC-1 with a purity of 98% was purchased from Sigma-Aldrich. Z-VAD-FMK with a purity of 95% was purchased from Santa Cruz Biotechnology (USA). The agents were dissolved in dimethyl sulfoxide (DMSO) at a concentration of 20 mM for Z-VAD-FMK and 50 mM for NEC-1.

Cell viability assay

Cell viability was quantified using the 3-(4,5-dimethylthiazol-2-yl)-2,5-diphenyltetrazolium bromide (MTT; Sigma-Aldrich) assay, as previously described (Hussein et al., 2016). Cell proliferation was determined using Ki-67 staining. The primary antibody against Ki-67 (1:400, #12202S; Cell Signaling Technology, USA) was used with the LSAB+ System-HRP kit (K0679; Dako, Denmark). Cell number was determined by hematoxylin staining (Park et al., 2016).

Cytotoxicity assays

miHeps and msHeps were treated with 20 μM Z-VAD-FMK or 50 μM NEC-1 for 48 h. The lactate dehydrogenase (LDH) assay (Promega Co., USA) was performed per the manufacturer's instructions. The absorbance was measured in a microplate reader (Thermo Scientific Multiskan Spectrum; Thermo Fisher Scientific) at 490 nm. The LDH release percentage was calculated from the maximum LDH release (100%) induced by lysing cells with 0.1% Triton X-100.

Quantitative polymerase chain reaction

Total RNA was isolated from cells and transcribed into cDNA using the NucleoSpin RNA Mini kit (Macherey-Nagel GmbH & Co., Germany) and TOPscrip RT DryMIX (Enzynomics, Korea), respectively, according to the manufacturer's instructions. Quantitative polymerase chain reaction (qPCR) was performed using TOPreal qPCR 2× PreMIX (Enzynomics) on a StepOnePlus real-time PCR system (Thermo Fisher Scientific). The relative expression was calculated by the comparative Ct ($2^{-\Delta\Delta Ct}$) method with glyceraldehyde 3-phosphate dehydrogenase (*GAPDH*) as the internal control. The primer sequences used were as follows: *ALB*, forward 5′-GACACCATGCCTGCTGATCT-3′, reverse 5′-CACGAGAGTTGGGGTTGACA-3′; *ASGPR1*, forward 5′-CCACATGGGCCCCTTAAACA-3′, reverse 5′-GGGTTTCAATACGCACCCCT-3′; *GAPDH*, forward 5′-CCTGCGACTTCAACAGCAAC-3′, reverse 5′-TGGGATAGGGCCTCTCTTGC-3′.

Immunoprecipitation and western blotting

Cells were washed with phosphate-buffered saline (PBS), lysed in mammalian lysis buffer (50 mM Tris-Cl, pH 8.0; 150 mM NaCl; 1 mM ethylenediaminetetraacetic acid; 1% NP-40; and 0.4 mM phenylmethylsulfonyl fluoride), sonicated, and centrifuged at 10,640 g for 10 min. For the immunoprecipitation assay, cell lysates were incubated for 4 h at 4℃ with rabbit anti-RIP3 antibody (1:1,000; Cell Signaling Technology) bound to protein A/G-agarose beads (Santa Cruz Biotechnology). Immunoprecipitated beads were washed 3 times with mammalian lysis buffer. Immunoprecipitates and whole-cell lysates were subjected to sodium dodecyl sulfate polyacrylamide gel electrophoresis, separated, and transferred to a polyvinylidene difluoride membrane. Blots were probed overnight with the appropriate dilutions of goat anti-albumin (ALB) antibody (1:2,000; Abcam), goat anti-HNF4 antibody (1:2,000; Santa Cruz Biotechnology), anti-actin-horseradish peroxidase (HRP) antibody (1:2,000; Santa Cruz Biotechnology), mouse anti-receptor-interacting protein kinase (RIP) antibody (1:1,000; BD Transduction Laboratories, USA), rabbit anti-RIP3 antibody (1:1,000; Cell Signaling Technology), rabbit anti-phospho-RIP3 antibody (1:1,000; Abcam), rabbit anti-caspase-3 antibody (1:1,000; Cell Signaling Technology), rabbit anti-cleaved-caspase-3 antibody (1:1,000; Cell Signaling Technology), and rat anti-MLKL antibody (1:1,000; Millipore, USA) at 4℃. Membranes were incubated with the respective HRP-conjugated secondary antibody (1:2,000; Santa Cruz Biotechnology). Membranes were then washed and developed with enhanced chemiluminescence western blotting detection reagents.

Albumin and urea secretion

Albumin and urea secretion in culture medium was analyzed using the Albumin ELISA Quantitation kit (Bethyl Laboratories, USA) and Urea Assay kit (Abcam).

Cell death assessment

Cell death was assessed by annexin V/propidium iodide (PI) staining. Phosphatidylserine expression, as an early sign of

apoptosis, was determined by fluorescence microscopy analysis through the binding of fluorescein isothiocyanate-labeled annexin V (Invitrogen, USA) to phosphatidylserine. PI was used to differentiate necrotic cells. Hoechst dye was used for nuclear staining. Fluorescence images were recorded using the IX-71-22FL/PH microscope (Olympus, Japan).

Measurement of ROS generation

The generation of ROS was measured using 2',7'-dichlorodihydrofluorescein diacetate (Invitrogen) as a substrate, according to the manufacturer's instructions. The absorbance was measured using the microplate reader at 520 nm.

Statistical analysis

Data are presented as the mean ± standard error of the mean (SEM). Statistical analysis was performed using two-way ANOVA, followed by Student's *t*-test.

RESULTS

Characteristics of miHeps

The viability of miHeps decreased at passage 14 (hepatocyte-like cells for 42 days), but the survival rate of msHeps did not change (Fig. 1A). In addition, miHeps released LDH from passage 14, but the cytotoxicity in msHeps did not change (Fig. 1B). Ki-67 staining was reduced in miHeps at passage 14 (Fig. 1C). miHeps showed decreased cell viability and increased cytotoxicity at passage 14.

We investigated the expression of albumin (ALB) as a liver function marker and that of surface receptor asialoglycoprotein receptor (ASGPR) as a mature hepatocyte marker (Kang et al., 2017). ALB expression in miHeps increased to 5.29 ± 2.0 at passage 10 and decreased to 0.12 ± 0.2 at passage 14 (Fig. 2A). ALB expression in msHeps decreased to 0.66 ± 1.4 and 0.80 ± 0.3 at passage 10 and passage 14, respectively. The expression of ASGPR in miHeps increased to 11.78 ± 0.1 at passage 10 and decreased to 0.82 ± 0.6 at passage 14 (Fig. 2A). The expression of ASGPR in msHeps increased to 4.20 ± 0.5 at passage 10 and decreased to 1.06 ± 0.2 at passage 14. ALB and HNF4α expression also increased at passage 10 and decreased at passage 14 in miHeps (Fig. 2B), whereas they did not change in msHeps. ALB secretion from miHeps increased at passage 10 and decreased at passage 14 (Fig. 2C), whereas it did not change in msHeps. Urea secretion in both miHeps and msHeps increased at passage 10 and decreased at passage 14 (Fig. 2D). miHeps lost hepatic function at passage 14.

Necroptosis of miHeps

Cell death was assessed by annexin V/PI staining. miHeps showed 4.8% annexin V-positive cells and 53% PI-positive cells at passage 14 (Fig. 3A). At passage 14, the proportion of annexin V-positive cells in msHeps was 1.3% and the proportion of PI-positive cells was 10%. We examined the expression of a necroptosis key protein, RIP1, and a key protein in apoptosis, caspase-3. Cleavage of caspase-3 was not observed in miHeps or msHeps, and the expression of RIP1, RIP3, phospho-RIP3 and MLKL increased only in miHeps at passage 14 (Fig. 3B). We also evaluated the binding of RIP1 and RIP3 to cells to determine whether necrosome for-

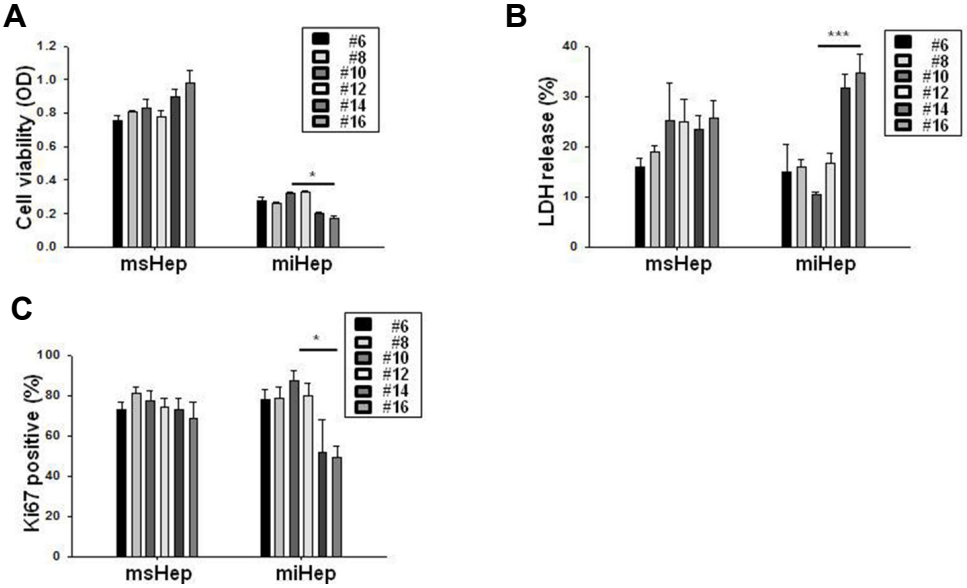

Fig. 1. Characterization of mouse induced hepatocyte-like cells. SV40-immortalized mouse hepatocytes (msHeps) and mouse induced hepatocyte-like cells (miHeps) from various passages were seeded at a density of 10,000 cells in 96-well plates for 48 h. (A) Cell proliferation was analyzed by the 3-(4,5-dimethylthiazol-2-yl)-2,5-diphenyltetrazolium bromide (MTT) assay. (B) Cytotoxicity was analyzed by the lactate dehydrogenase (LDH) test. The percentage of LDH was calculated from the maximum LDH release (100%) induced by lysing cells with 0.1% Triton X-100. (C) Cell viability was evaluated by Ki-67 immunohistochemistry. Data are expressed as the mean ± SEM; $*P < 0.05$, and $***P < 0.001$ from three independent experiments.

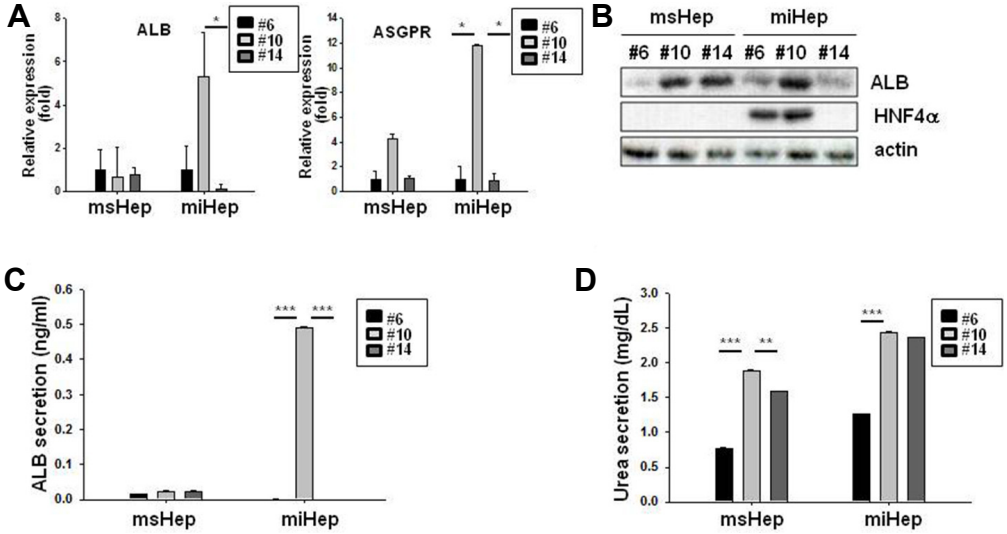

Fig. 2. Hepatic function in miHeps. msHeps and miHeps from various passages were cultured for 48 h. (A) Expression of genes specific for albumin (*ALB*) and asialoglycoprotein receptor (*ASGPR*) in msHeps and miHeps was determined using quantitative polymerase chain reaction and normalized to the expression of glyceraldehyde 3-phosphate dehydrogenase (*GAPDH*). (B) msHep and miHep lysates were subjected to western blot analysis with anti-ALB and anti-hepatocyte nuclear factor 4 alpha (HNF4α) antibodies. Actin was used as a loading control. (C) ALB and (D) urea secretion in the cell culture medium was analyzed by enzyme-linked immunosorbent assay (ELISA). Data are expressed as the mean ± SEM; *P < 0.05, **P < 0.01, and ***P < 0.001 from three independent experiments.

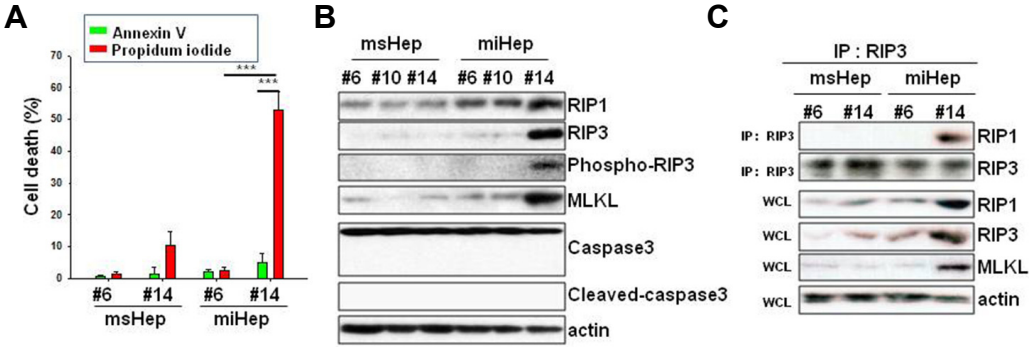

Fig. 3. miHeps underwent necroptotic cell death. msHeps and miHeps from passage 6 and passage 14 were cultured for 48 h. (A) msHeps and miHeps were stained with annexin V (green), propidium iodide (PI) (red), and Hoechst 33342 (blue), and analyzed with a fluorescence microscope. The percentage of PI- or annexin V-positive cells with blue nuclear stain was determined by counting at least 300 cells from 3 independent experiments. Data are expressed as the mean ± SEM; ***P < 0.001 from three independent experiments. (B) msHep and miHep lysates were subjected to Western blot analysis with the indicated antibodies. Actin was used as a loading control. (C) msHep and miHep lysates were co-immunoprecipitated with anti-RIP3 antibody and subjected to Western blotting analysis. IP, immunoprecipitation; WCL, whole cell lysate.

mation occurred. RIP1 and RIP3 bound to miHeps at passage 14 (Fig. 3C). miHeps died because of necrosome formation and necroptosis.

NEC-1 inhibited necroptosis in miHeps

NEC-1 was used to examine the cell death of miHeps. Z-VAD-FMK was used as a control (Masuoka et al., 2009). To determine the concentration of NEC-1, cell viability and cytotoxicity assays were performed. NEC-1 was used at 50 μM (Supplementary Figs. 1A and 1B) because it was cytotoxic at 100 μM, although cell survival was not affected at high concentrations. The effect of MTT was not statistically significant. Effects of NEC-1 on cell death were confirmed by annexin V and PI staining. The proportion of annexin V-positive cells in miHeps at passage 14 treated with vehicle (DMSO) was 3.6%, and that of PI-positive cells was 29.5%. In NEC-1-treated miHeps at passage 14, the percentage of annexin V-positive cells was 2.5%, and that of PI-positive cells was 1.1% (Fig. 4A). Thus, NEC-1 inhibited necroptosis in miHeps. To determine the effect of NEC-1 on cell viability, the MTT

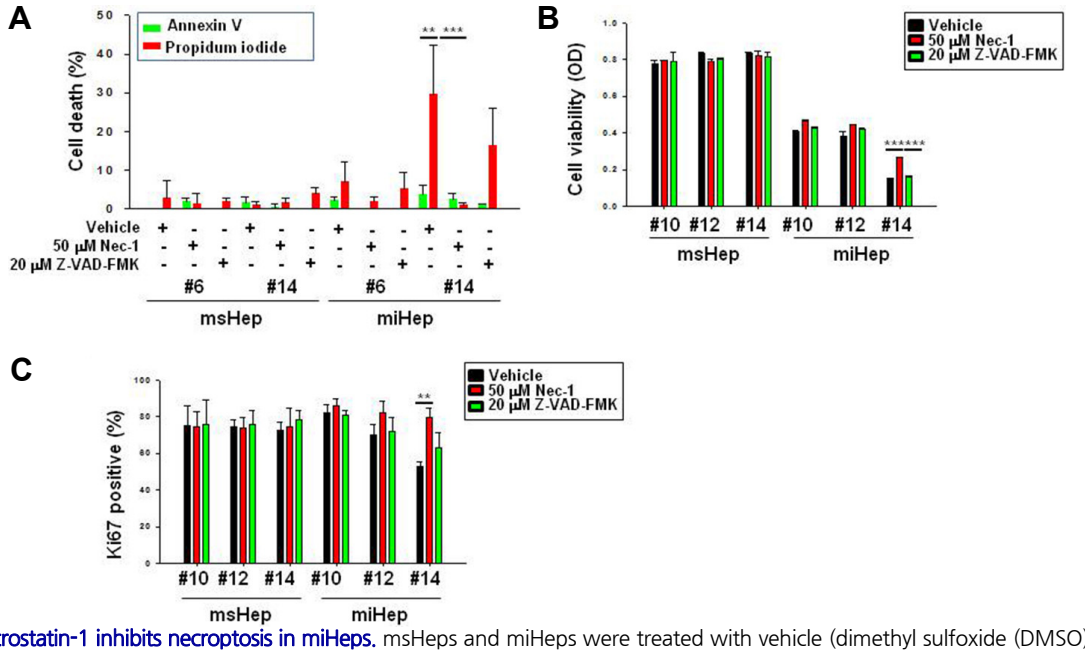

Fig. 4. Necrostatin-1 inhibits necroptosis in miHeps. msHeps and miHeps were treated with vehicle (dimethyl sulfoxide (DMSO)), 50 μM necrostatin-1 (NEC-1), or 20 μM Z-VAD-FMK. (A) Cells were stained with annexin V (green), PI (red), and Hoechst 33342 (blue), and analyzed with a fluorescence microscope. The percentage of PI- or annexin V-positive cells with blue nuclear staining was determined by counting at least 300 cells from 3 independent experiments. (B) Cell proliferation was analyzed by the MTT assay. (C) Cell viability was evaluated by Ki-67 immunohistochemistry. Data are expressed as the mean ± SEM; $^{**}P < 0.01$, and $^{***}P < 0.001$ from three independent experiments.

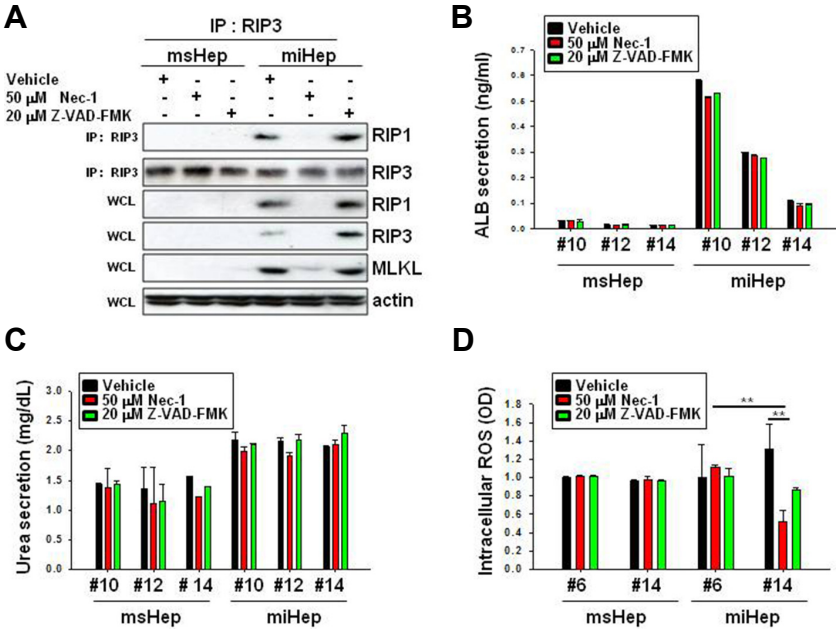

Fig. 5. NEC-1 inhibits reactive oxygen species formation and suppresses miHep cell death. msHeps and miHeps were treated with vehicle (DMSO), 50 μM NEC-1, or 20 μM Z-VAD-FMK. (A) Cell lysates from passage 14 were co-immunoprecipitated with anti-RIP3 antibody, and western blot analysis was performed using the indicated antibodies. IP, immunoprecipitation; WCL, whole cell lysate. (B) ALB and (C) urea secretion in the cell culture medium was analyzed by ELISA. (D) Intracellular reactive oxygen species (ROS) were measured by ELISA. Data are expressed as the mean ± SEM; $^{**}P < 0.01$ from three independent experiments.

assay and Ki-67 staining were performed. At passage 14, the OD of miHeps was 0.15 with vehicle treatment and 0.27 with NEC-1 treatment (Fig. 4B). In addition, at passage 14, 53% of miHeps were stained with Ki-67 after vehicle treatment and 79% of miHeps were stained with Ki-67 after NEC-1 treatment (Fig. 4C). msHeps did not change during treatment with NEC-1 and Z-VAD-FMK. Thus, NEC-1 increased the survival of miHeps.

NEC-1 inhibited necroptosis by inhibiting ROS generation without affecting the hepatic function of miHeps

To determine the mechanism underlying the prevention of cell death by NEC-1 in miHeps, we evaluated whether NEC-1 inhibited necrosome formation. RIP1 and RIP3 bound to the vehicle at passage 14 in miHeps, but they did not bind to NEC-1 (Fig. 5A). Thus, NEC-1 inhibited necrosome formation in miHeps.

We examined ALB secretion in miHeps and showed that it did not change at passages 10, 12 and 14 during vehicle, NEC-1, or Z-VAD-FMK treatment (Fig. 5B). Urea secretion also did not change during any of the treatments (Fig. 5C). ALB and HNF4α expression did not change in miHeps during vehicle, NEC-1, or Z-VAD-FMK treatment (Sup. 2). NEC-1 did not affect the hepatic function of miHeps. We evaluated whether NEC-1 inhibited ROS formation in miHeps. miHeps increased ROS generation under vehicle treatment at passage 14 but inhibited ROS generation under NEC-1 treatment (Fig. 5D). We conclude that NEC-1 inhibited necrosome formation, ROS generation, and necroptosis in miHeps.

DISCUSSION

In this study, miHeps bound to RIP1 and RIP3, which are associated with necrosome formation, suggesting that these cells underwent necroptosis. Treatment with NEC-1 increased miHep survival, did not promote binding to RIP1 and RIP3, inhibited ROS formation, and inhibited necroptosis.

Necroptosis causes hepatocellular inflammation and hepatic lesions such as those in fulminant hepatic failure (FHF), acute liver failure (ALF), non-alcoholic fatty liver disease (NAFLD), and excessive acetaminophen use (APAP) (Afonso et al., 2015; Kim and Lee, 2017; Seo et al., 2017; Takemoto et al., 2014). Necroptosis is caused by necrosomal RIP kinase 1 (RIPK1) and RIPK3, which are regulated by their ubiquitination and phosphorylation (Takemoto et al., 2014). Here, we described that the mechanism underlying the death of miHeps involves RIP1/RIP3 binding and sub-stage MLKL activation without caspase activation (Figs. 3B and 3C). Hepatocyte-like cells derived from iPSCs (iPSC-Heps) from fibroblasts of patients with Alpers-Huttenlocher syndrome are known to undergo mitochondrial-dependent cell death associated with caspase-9 and cytochrome c release induced by valproic acid (Li et al., 2015). Therefore, further investigation is needed on the mechanism of the death of reprogrammed hepatocytes in other tissues.

NEC-1 strongly inhibits hepatic damage and hepatocyte-specific interleukin 33 (IL-33) expression in the liver *in vivo* and in hepatic stellate cells (Arshad et al., 2015). It also reduces the expression of NLRP3, ASC, caspase-1 and inflammatory component proteins as well as serum IL-1β levels in the ALF model (Seo et al., 2017). NEC-1 decreases the amount of ROS produced in APAP-damaged hepatocytes, whereas the depletion of cytochrome P450 2E1 (CYP2E1) and total glutathione levels are not affected (Takemoto et al., 2014). In our study, miHeps treated with NEC-1 showed increased survival, no binding to RIP1 or RIP3, inhibition of ROS formation, and inhibition of necroptosis. However, NEC-1 did not affect urea or ALB secretion.

When iHeps were cultured in 3D hydrogels, ALB and urea secretion, glycogen synthesis, and cytochrome P450 (CYP450) activity compared to that in 2D culture (Luo et al., 2017). In addition, when iHeps were cultured on a liver-derived extracellular matrix scaffold, they showed increased CYP450 (CYP2C9, CYP3A4, and CYP1A2) mRNA levels and enzyme activity compared to culture in a Matrigel sandwich or bioplotted poly-L-lactic acid, leading to hepatocyte maturation (Wang et al., 2016). Therefore, the miHeps used in this study require additional 3D culture experiments. Hepatocytes that can be used in an artificial liver have not yet been optimized. The miHep necroptosis mechanism provides information on liver cells that may be used for generating artificial livers. In addition, the protection of miHeps against cell death mediated by NEC-1 may provide useful information for the use of hepatocytes in developing artificial livers. Therefore, our future research will focus on hepatocyte cells with enhanced survival and hepatic function.

Note: Supplementary information is available on the Molecules and Cells website (www.molcells.org).

ACKNOWLEDGMENTS

This work was supported by the "Cooperative Research Program for Agriculture Science & Technology Development (Project No. PJ01100201)" Rural Development Administration, Republic of Korea.

REFERENCES

Afonso, M.B., Rodrigues, P.M., Carvalho, T., Caridade, M., Borralho, P., Cortez-Pinto, H., Castro, R.E., and Rodrigues, C.M. (2015). Necroptosis is a key pathogenic event in human and experimental murine models of non-alcoholic steatohepatitis. Clin. Sci. *129*, 721-739.

Arshad, M.I., Piquet-Pellorce, C., Filliol, A., L'Helgoualc'h, A., Lucas-Clerc, C., Jouan-Lanhouet, S., Dimanche-Boitrel, M.T., and Samson, M. (2015). The chemical inhibitors of cellular death, PJ34 and Necrostatin-1, down-regulate IL-33 expression in liver. J. Mol. Med. *93*, 867-878.

Cho, Y.S. (2014). Perspectives on the therapeutic modulation of an alternative cell death, programmed necrosis (review). Int. J. Mol. Med. *33*, 1401-1406.

Cho, Y.S., and Park, H.L. (2017). Exploitation of necroptosis for treatment of caspase-compromised cancers. Oncol. Lett. *14*, 1207-1214.

Dasarathy, S. (2012). Consilience in sarcopenia of cirrhosis. J. Cachexia, Sarcopenia Muscle *3*, 225-237.

Dienstag, J.L., and Cosimi, A.B. (2012). Liver transplantation--a vision realized. N. Eng. J. Med. *367*, 1483-1485.

Hannoun, Z., Steichen, C., Dianat, N., Weber, A., and Dubart-Kupperschmitt, A. (2016). The potential of induced pluripotent stem cell derived hepatocytes. J. Hepatol. *65*, 182-199.

Ho, C.M., Lee, P.H., Cheng, W.T., Hu, R.H., Wu, Y.M., and Ho, M.C. (2016). Succinct guide to liver transplantation for medical students. Ann. Med. Surg. *12*, 47-53.

Hussein, K.H., Park, K.M., Kang, K.S., and Woo, H.M. (2016). Heparin-gelatin mixture improves vascular reconstruction efficiency and hepatic function in bioengineered livers. Acta Biomater. *38*, 82-93.

Kang, K., Kim, Y., Lee, S.B., Kim, J.S., Park, S., Kim, W.D., Yang, H.M., Kim, S.J., Jeong, J., and Choi, D. (2017). Three-dimensional bioprinting of hepatic structures with direct-converted hepatocyte-like cells. Tissue Engineering. Part A.

Kim, S.J., and Lee, S.M. (2017). Necrostatin-1 Protects Against D-Galactosamine and Lipopolysaccharide-Induced Hepatic Injury by Preventing TLR4 and RAGE Signaling. Inflammation *40*, 1912-1923.

Leberfinger, A.N., Ravnic, D.J., Dhawan, A., and Ozbolat, I.T. (2017). Concise review: bioprinting of stem cells for transplantable tissue fabrication. Stem Cells Transl. Med. *6*, 1940-1948.

Li, S., Guo, J., Ying, Z., Chen, S., Yang, L., Chen, K., Long, Q., Qin, D., Pei, D., and Liu, X. (2015). Valproic acid-induced hepatotoxicity in Alpers syndrome is associated with mitochondrial permeability transition pore opening-dependent apoptotic sensitivity in an induced pluripotent stem cell model. Hepatology *61*, 1730-1739.

Luo, Y., Lou, C., Zhang, S., Zhu, Z., Xing, Q., Wang, P., Liu, T., Liu, H., Li, C., Shi, W., et al. (2017). Three-dimensional hydrogel culture conditions promote the differentiation of human induced pluripotent stem cells into hepatocytes. Cytotherapy 20, 95-107.

Masuoka, H.C., Guicciardi, M.E., and Gores, G.J. (2009). Caspase inhibitors for the treatment of hepatitis C. Clin. Liver Dis. *13*, 467-475.

Park, K.M., Hussein, K.H., Hong, S.H., Ahn, C., Yang, S.R., Park, S.M., Kweon, O.K., Kim, B.M., and Woo, H.M. (2016). Decellularized liver extracellular matrix as promising tools for transplantable bioengineered liver promotes hepatic lineage commitments of induced pluripotent stem cells. Tissue Eng. Part A *22*, 449-460.

Sakiyama, R., Blau, B.J., and Miki, T. (2017). Clinical translation of bioartificial liver support systems with human pluripotent stem cell-derived hepatic cells. World J. Gastroenterol. *23*, 1974-1979.

Seo, M.J., Hong, J.M., Kim, S.J., and Lee, S.M. (2017). Genipin protects d-galactosamine and lipopolysaccharide-induced hepatic injury through suppression of the necroptosis-mediated inflammasome signaling. Eur. J. Pharmacol. *812*, 128-137.

Takemoto, K., Hatano, E., Iwaisako, K., Takeiri, M., Noma, N., Ohmae, S., Toriguchi, K., Tanabe, K., Tanaka, H., Seo, S., et al. (2014). Necrostatin-1 protects against reactive oxygen species (ROS)-induced hepatotoxicity in acetaminophen-induced acute liver failure. FEBS Open Bio. *4*, 777-787.

Wang, B., Jakus, A.E., Baptista, P.M., Soker, S., Soto-Gutierrez, A., Abecassis, M.M., Shah, R.N., and Wertheim, J.A. (2016). Functional maturation of induced pluripotent stem cell hepatocytes in extracellular matrix-A comparative analysis of bioartificial liver microenvironments. Stem Cell Transl. Med. *5*, 1257-1267.

Wang, Y., Nicolas, C.T., Chen, H.S., Ross, J.J., De Lorenzo, S.B., and Nyberg, S.L. (2017). Recent advances in decellularization and recellularization for tissue-engineered liver grafts. Cells Tissues Organs *204*, 125-136.

Zarrinpar, A., and Busuttil, R.W. (2013). Liver transplantation: past, present and future. Nat. Rev. Gastroenterol. Hepatol. *10*, 434-440.